INTERNATIONAL ATOMIC ENERGY AGENCY
UNITED NATIONS EDUCATIONAL, SCIENTIFIC AND CULTURAL ORGANIZATION

INTERNATIONAL CENTRE FOR THEORETICAL PHYSICS
34100 TRIESTE (ITALY) - P.O.B. 586 - MIRAMARE - STRADA COSTIERA 11 - TELEPHONE: 2240-1
CABLE: CENTRATOM - TELEX 460892-1

H4.SMR/167 - 5

SCHOOL ON PHYSIC IN INDUSTRY

27 January - 14 February 1986

---

# PHYSICS IN COMPUTER INDUSTRY

presented by

S. TRIEBWASSER
IBM - T.J. Watson Research Center
89-N16
P.O. Box 218
Yorktown Heights, NY 10598
U.S.A.

---

## General Outline

Physicists and Career Paths

Physics Research in the Computer Industry

Review of Some Specific Projects



## Publications

1953: Fine Structure of Hydrogen, PR

1955: Phase Diagram of KNbO3/KTaO3 J. Am. Chem. Soc.

1957: Free Energy and Internal Fields in BaTiO3, J. Phys. Chem.

1959: Study of Ferroelectric Transition in Mixed Niobates, PR

1963: Quantum Efficiency of GaAs Injection Lasers, Appl. Phys. Ltrs.

1964: Effect of Surface Scattering on Mobility in Surface Inversion Layers in Si, Phys. Ltrs.

1969: LSI and the Revolution in Electronics, Science

1983: VLSI in High End Systems, AFRICON 83

esearch in Representative Companies

NEC
- Si Etching Mechanisms
- Mo and SiO2 Sputtering
- Si on Insulators
- Mo silicide properties
- Si Oxidation

Xerox
- Crystal Growth
- Film Properties
- Surface Science
- Photo Emission
- Extensive III–V Work
- Crystal Defects
- Magneto Optics
- Polymer Physics
- Amorphous Silicon
- Non-Linear Phenomena

Hitachi
- Si and GaAs Device Physics
- Josephson Junctions
- Aharanov-Bohm Effect
- Lithography Physics

Hewlett Packard
- Frequency Standards
- X-ray and E Beam Lithography
- Surface Acoustic Waves

Siemens
- Device Physics, GaAs, Si
- Lasers
- Nuclear Magnetic Resonance

Texas Instruments
- Spatial Quantization
- Device Limits
- Materials and Process Research

Sperry
- Josephson Tunneling
- Hetero-structures
- Si Microstructures

Honeywell
- GaAs Devices
- Holography

Honeywell Bull
- Hot Electrons in Si Devices
- Magnetic Properties of Alloys

4

Hewlett Packard

are increasingly attractive in commercial products. I will also not discuss the important area of sensors, although it is still the bottleneck in many situations. Innovation in this area is steady but slow; cost, reliability, performance, and size of sensors are often limiters to the application of digital technology to measurement and test applications.

Let us first consider the impact of computers and digital signal processing on precision measurements. Since 1967 the world's time has been regulated by commercially available cesium beam atomic clocks to an accuracy of 1 s in 100,000 years, or about 3–5 parts in $10^{12}$. Incredible as this may seem, it is not good enough for many modern navigation, communication, and astronomical applications. Len Cutler and his group at HP Laboratories, who developed the HP cesium standard that is in wide use throughout the world, have demonstrated an elegant new technique that is about 10 times more accurate, based on the hyperfine transitions of trapped mercury ions. Ideally, an atomic frequency standard is based on the electric or magnetic dipole transition of a free atom observed for an infinite amount of time. In the cesium standard, the ideal of the free atom is realized to a high degree, but the observation time (i.e., the time of flight through a microwave cavity) is fairly short.

Figure 1 shows the experimental apparatus designed to overcome this limitation. Mercury 199 ions are trapped for long periods in a quadrupole configuration driven by a precisely calculated radio-frequency field. The ions are pumped to an excited state using Mercury 202 light, and then irradiated with the microwave frequency tuned first to one side of the resonance at 40.5 GHz and then to the other. The counter signals derived from the fluorescence that results are differenced and digitally integrated by the computer, using second differencing methods, and are then converted to an analog signal. If the mean frequency of the microwave source is not at the line center, the error signal can be fed back, after a second integration, to a voltage controlled crystal oscillator, which in turn regulates the frequency source. Complex control sequences minimize the noise due to secondary effects, and careful attention must be paid to other noise sources, such as second order Doppler shift. Figure 2 indicates the results: The transition has been measured to an accuracy of 2 parts in $10^{11}$, with a line width of 0.85 Hz at 40.5 GHz. If the full width at half-maximum of this transition is depicted as 1 in. wide, then the origin is three times the distance to the moon! The servo signal derived from this yields an absolute accuracy conservatively estimated as 3 parts in $10^{13}$, or about 1 s per million years. It is remarkable that today only a garden variety microprocessor and high-speed microelectronics are all that are needed to make such elegant instrumentation

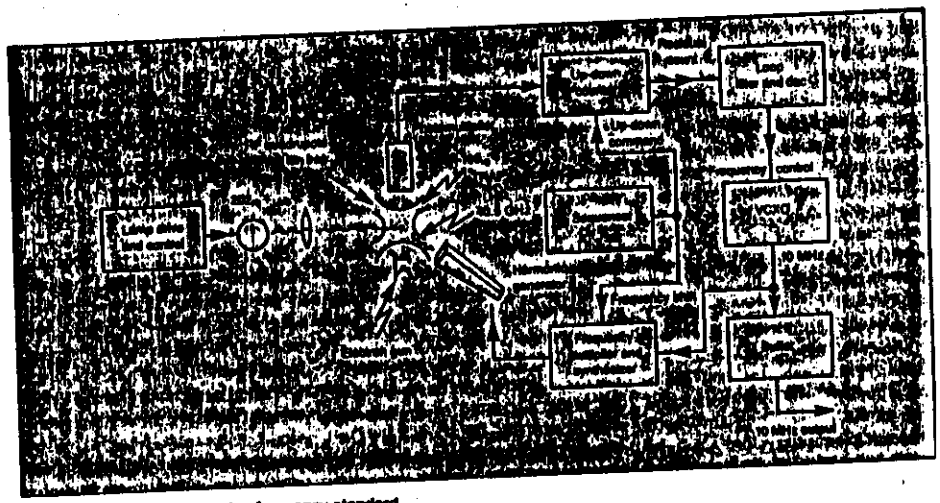

Figure 1. Trapped mercury ion frequency standard.



Joel Birnbaum

practical. Although the precision here is an extreme case, many modern instruments are based on this kind of digital control and processing capability, which was unthinkable just a few decades ago.

We can find some far less exotic examples in the nearest computer store. A best-selling program, Typing Master, available now for home computers, analyzes the user's performance on some typing assignments and provides immediate feedback on improvements of a very specific sort. Even lifelong professional typists learn immediately and interactively how to improve their speed or accuracy or both. Extension to many other skills by replacing the keyboard with a sensor is possible. For example, one-chip signal processors could soon provide useful biofeedback to people learning to sing or to play musical instruments, helping with the difficult-to-teach relationships between anatomical control and auditory phenomena. We will be able to see on a screen in real time the spectrum by octaves of the sound that is produced. Visual feedback of auditory phenomena can show dynamically the relationship of harmonics to the fundamental or the transitions between head and chest resonances, for example, in a way that our ears, which are not Fourier's children, cannot. Such equipment will enable singers and musicians to compare sound patterns and rhythms with stored templates produced by master musicians or with their own earlier efforts. The cost should be low enough to teach school children in the home. Programs to analyze speech accents and cadences are further in the future, but certainly possible. Similar techniques with different sensors will permit the semiautomatic tuning of instruments like pianos and Porsches.

Another type of personal computer program now becoming popular is the kit, like the Pinball Construction Set. Using simple pictorial interfaces and pointers, objects (in this case flippers, bumpers, spinners, bonus lights, etc.) are selected by the user from a pictorial menu, moved about on a screen, and assembled according to the rules that have been previously embedded in the kit by its creator. Many parameters in the pinball program can be changed—the location and elasticity of the bumpers and flippers, bonus-point combinations, etc. Items difficult to change on real pinball machines could also be modifiable: nonphysical gravitational fields, balls of arbitrary cross section, etc. After the almost infinitely variable game has been designed *without writing a single line of code*, it can be played immediately and further modified by the user. The output of the program is the pinball game. A later version of this idea involves a music-construction kit. The objects now are notes, score markings, tempi, etc. We can create melodies, snip them with iconic scissors, combine them with preprogrammed melodies, transpose to new keys, and so forth with no programming. The application is music composition, and the output of the program will be the score of the music itself. We will be able to play the results on conventional instruments or directly on electronic instruments if we desire.

This entire notion of kits seems to me a very powerful one. If the appropriate sets of rules of combination—the constraints—can be embedded in the machine by experts, then design can become possible based only on function and aesthetics for a vastly greater proportion of our population than is now possible. Consider an amateur architect designing an addition to his or her house using such techniques. The cost, the structural fac-

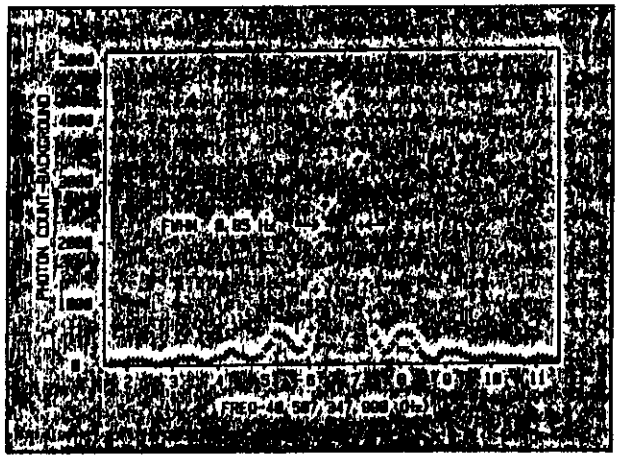


Figure 2. $199_{Hg}^{+}$ hyperfine resonance.

SPERRY

| | |
|---|---|
| Josephson Technology | - Materials and processes |
| Hetero Structures | - AlGaAs, GaInAs, etc.<br>- MODFET materials, processes<br>- MBE, OMVPE<br>- Quantum Well Devices<br>- Device Modelling<br>- Transport Mechanism |
| Silicon | - 0.5 and 0.25um devices<br>- E-Beam and x-ray processes, resists and masks<br>- Device models<br>- Low temperature operations<br>- Radiation hardness |
| Others | - Optical detectors<br>- Magnetic bubbles<br>- Optical storage<br>- Wafer Scale Packaging, etc. |

| | Ph.D.'s | %Physics |
|---|---|---|
| All IBM: | 3278 | 19.2 |
| Research: | 1012 | 26.3 |

tremely sensitive to the distance between the tip and the surface. A change in the distance by an amount equal to the diameter of a single atom causes the tunneling current to change by a factor of as much as 1,000.

We exploit the sensitivity of the tunneling current to produce exquisitely precise measurements of the vertical positions of the atoms on the sample's surface. As the tip is swept across the surface a feedback mechanism senses the tunneling current and maintains the tip at a constant height above the surface atoms. In this way the tip follows the contours of the surface. The motion of the tip is read and processed by a computer and displayed on a screen or a plotter. By sweeping the tip through a pattern of parallel lines a three-dimensional image of the surface is obtained. A distance of 10 centimeters on the image represents a distance of 10 angstroms on the surface: a magnification of 100 million.

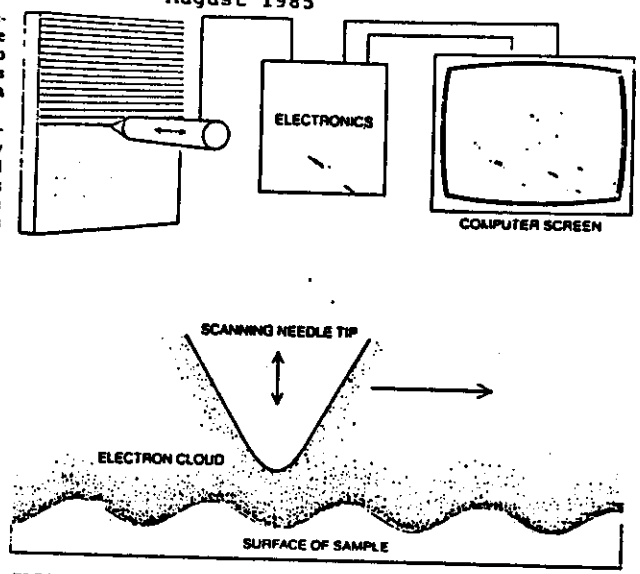


**ELECTRON TUNNELING** is the phenomenon that underlies the operation of the microscope. An electron cloud occupies the space between the surface of the sample and the needle tip (*bottom*). The cloud is a consequence of the indeterminacy of the electron's location (a result of its wavelike properties): because the electron is "smeared out," there is a probability that it can lie beyond the surface boundary of a conductor. The density of the electron cloud decreases exponentially with distance. A voltage-induced flow of electrons through the cloud is therefore extremely sensitive to the distance between the surface and the tip. As the tip is swept across the surface a feedback mechanism senses the flow (called the tunneling current) and holds constant the height of the tip above the surface atoms (*top*). In this manner the tip follows the contours of the surface. The motion of the tip is read and processed by a computer and displayed on a screen or a plotter. Sweeping the tip through a pattern of parallel lines yields a high-resolution, three-dimensional image of the surface.

How is it possible to move the needle over a sample while maintaining a gap between the tip and the surface that is less than 10 angstroms and achieve a stability and precision that is better than .1 angstrom? First, the microscope must be shielded from vibrations such as those caused by sound in the air and by people walking around in a building. Second, the drives of the needle must be highly precise. Finally, the tip must be as sharp as the limits of rigidity and stability allow.

Two stages, or sections, suspended from springs, nestle within the stainless-steel cylindrical frame of the microscope and protect the tunneling gap from vibration. Both stages, triangular in cross section, are made of glass rods. The second stage slips into the first stage, from which it is suspended by three springs. The first stage in turn is suspended from the outer frame, also by three springs. The second stage carries the heart of the microscope: it contains both the sample and the scanning needle.

When the entire microscope sits in a vacuum, air resistance is minimal and the first and second stages could, if they were disturbed, bounce up and down almost indefinitely. To stop this motion we rely on the phenomenon of eddy-current damping. We let copper plates attached to the bottom of the first and second stages slide between magnets attached to the outer frame. As each plate slides up and down, the magnetic field causes the conducting electrons of the copper to move around, inducing a so-called eddy current. The reaction between the eddy current and the magnetic field retards the motion of the plate and thereby protects the microscope from even the smallest vibrations.

Once the gross vibrations have been stopped the sample can be positioned. This is done with a specially developed drive that carries the sample across a horizontal metal plate on the second stage. The body of the drive consists of a slab of piezoelectric material that expands or contracts when voltage is applied. The drive has three metallic feet, arranged in triangular fashion, that are coated with a thin layer of insulating material. They can be clamped to the metal plate by establishing a voltage between them and the metal plate.

We move the drive in the following manner. Suppose, for instance, we clamp only one foot and apply a voltage to the piezoelectric body so that it contracts. The other two feet will move slightly. We then clamp those two feet, release the third foot and remove the applied voltage so that the body expands back to its original size. The drive has just moved one step. The step width can be varied between 100 and 1,000 angstroms. Since the drive can rotate about each of its feet, it can walk along the plate in any desired direction.

When the drive has carried the sample to the wanted tunneling position, we begin scanning the surface of the sample. We use a rigid tripod made of three piezoelectric sticks to move the tip of the scanning needle. When we apply a voltage to expand or contract one of the sticks, the other two bend slightly. Consequently the tip moves in a straight line over distances as great as 10,000 angstroms. Furthermore, this motion is quite sensitive to the magnitude of the applied voltage: a voltage on the order of .1 volt results in a motion of 1.0 angstrom. The precision of the tripod's drive is so good that at present only vibration limits the vertical resolution of the sample's surface. This resolution at present is in the

(MORE)



range of approximately a few hundredths of an angstrom.

The lateral resolution of the surface is limited by the sharpness of the tip. In this instance nature has been kind to the vacuum tunneler. It is relatively easy to make a sharp tip that yields a lateral resolution of about six to 12 angstroms: one simply grinds the end of a needle, which is usually made of tungsten.

To achieve a lateral resolution of two angstroms, however, the needle must have a single atom sitting securely on top of its tip. Such an atom usually comes from the sample itself. It is dislodged by high electric fields that are caused by applying a voltage difference of from two to 10 volts between the sample and the tip. Since luck plays a large role in the final stage, we are trying to sharpen the tip by bombarding it with a high-energy beam of ions. This causes the atoms on the surface to sputter away in a highly controlled manner.

In addition to delineating the atomic topography of a surface, the scanning tunneling microscope reveals atomic composition. The tunneling current depends both on the tunnel distance and the electronic structure of the surface and on the fact that each atomic element has an electronic structure uniquely its own.

The ability of the microscope to resolve both topography and electronic structure will make it useful to investigators in physics, chemistry and biology. We first pursued the simplest case: the topographic structures of single crystals characterized by a homogeneous surface structure. Crystals consist of identical atomic layers built one on top of another. While results from scattering experiments indicate that the top layer is different from and more complex than the others, the precise structure of this layer was hard to determine.

The best-known surface structure is the diamond-shaped unit cell of silicon. Since each of the four edges of the cell measures seven atomic spacings, the cell is referred to as the 7-by-7. Each 7-by-7 contains 12 bumps that have not been visualized before. Each bump apparently corresponds to a single atom. The arrangement of the surface atoms is, although aesthetically pleasing, quite complex. This is in contrast to the relatively simple structure of any bulk layer found in silicon. Its unit cell, 49 times smaller in area than the 7-by-7, contains only two atoms. Another great difference between the two kinds of layers is that the surface layer is much rougher than any bulk layer. Although the surface pattern is now known and a vast amount of information about it has been gained from other experiments, the reason this and not a different structure forms is not yet understood.

Another crystal whose surface structure is now better understood is the gold crystal. We found that when we cut the crystal in a direction parallel to its atomic layers, the resulting face is smooth. A cut in a direction diagonal to the atomic layers results in a rougher face. Just as one learns from studying the earth's crust how it was formed millions of years ago, so we have learned from studying these surfaces how they took shape. Current theories reveal that the diagonally cut surface assumes its jagged nature because such a configuration has a lower energy and is consequently stabler than a smooth configuration.

A more exotic branch of physics, the study of superconductivity, has also benefited from the application of scanning tunneling microscopy. A superconducting material is characterized by its complete lack of electrical resistance. The use of superconductors to make cables that are free from power losses could save enormous amounts of energy. The colliding-beam acceler-

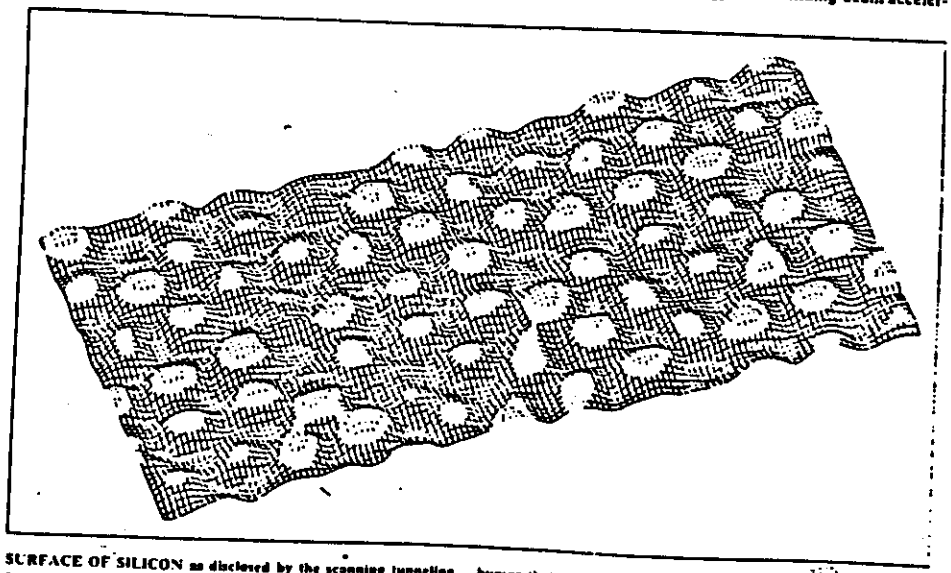

**SURFACE OF SILICON** as disclosed by the scanning tunneling microscope consists of a pattern of diamond-shaped unit cells. Each cell measures 27 angstrom units (one angstrom unit is one ten-billionth of a meter) on a side. The cell is called the *7-by-7* because each side measures seven atomic units. Each 7-by-7 contains 12 bumps that are arranged in two groups of six. The bumps, which have never before been resolved, apparently correspond to the surfaces of individual atoms. They stand as much as 1.3 angstroms above the rest of the surface. The image was formed by applying a voltage so that electrons flowed from the needle tip to the surface.

(MORE)

# Partitioning Problem

1000 Logic Gates

2 Chips

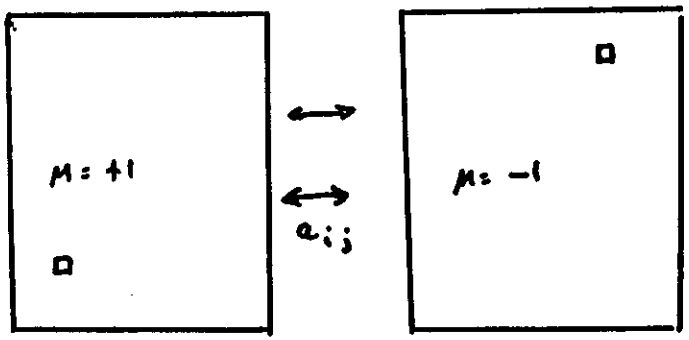




## Objective Function for Partition

example: partition into two classes, connectivity given

( $a_{ij}$ = no. of wires linking object i to object j)

( $\mu_i = \pm 1$)

**Objective function:**

f = total crossing wires + $\lambda$ * imbalance$^2$

$$= \sum_{i<j} (a_{ij}/4)(\mu_i - \mu_j)^2 + \lambda * \left(\sum_i \mu_i\right)^2$$

$$= \text{constant} + \sum_{i<j} (\lambda - a_{ij}/2)\,\mu_i \mu_j$$

CDG 1/23/81

## Metropolis Monte Carlo Algorithm

**Four Ingredients:**

1) Means of defining configurations $C_i$

2) Scalar objective function, $E(C_i)$, to quantify tradeoffs

3) Mechanism for generating random local changes in configuration

4) Annealing schedule

**Algorithm:**

Propose a configuration change from $C_i$ to $C_j$

Calculate change in objective function,

$\Delta E = E(C_j) - E(C_i)$

Accept new configuration with probability P

$= 1$ if $\Delta E < 0$

$= \exp(-\Delta E/T)$ if $\Delta E > 0$

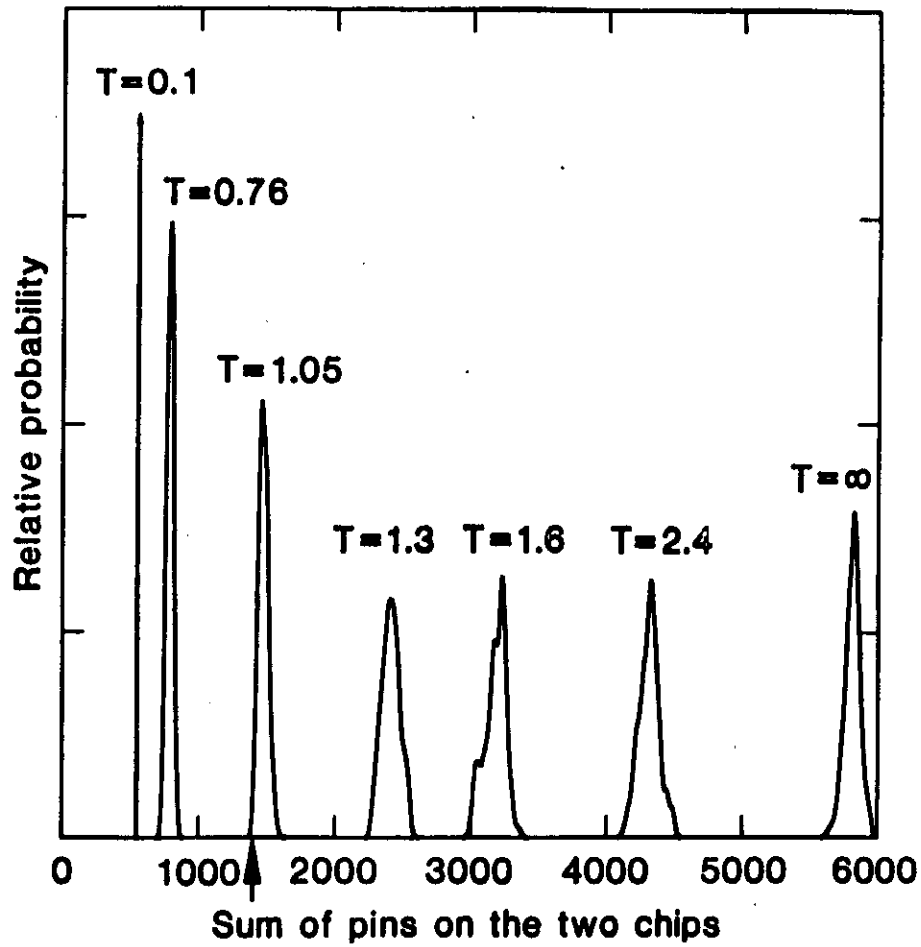


CDG
4/8/81

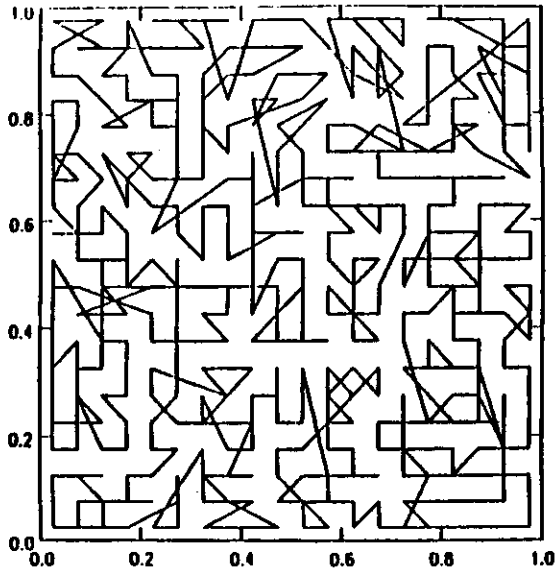


400 pts
T = 1.0
ℓ = 1.85

FIGURE 1A

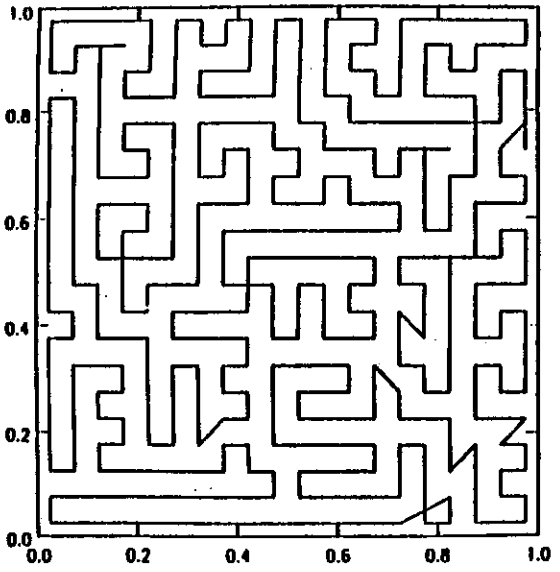


400 pts
T = 0.3
ℓ = 1.04

FIGURE 1B

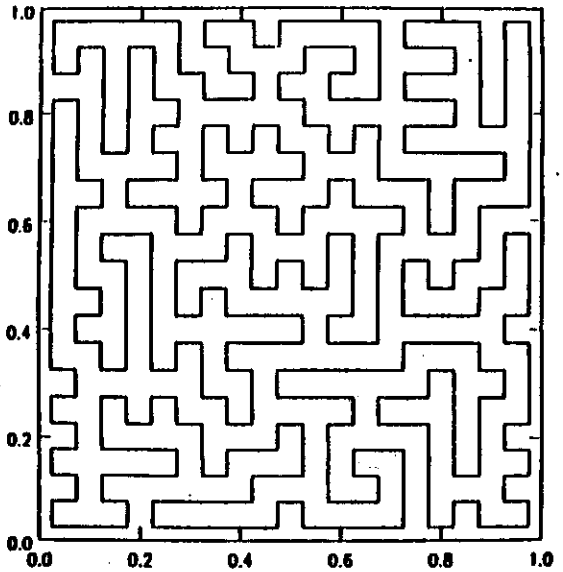


400 pts
T = 0
ℓ = 1

FIGURE 1C

1a - c. Travelling salesman tours obtained by simulated annealing at temperatures (a) T = 1.0, (b) T = 0.3, and (c) T = 0.0.

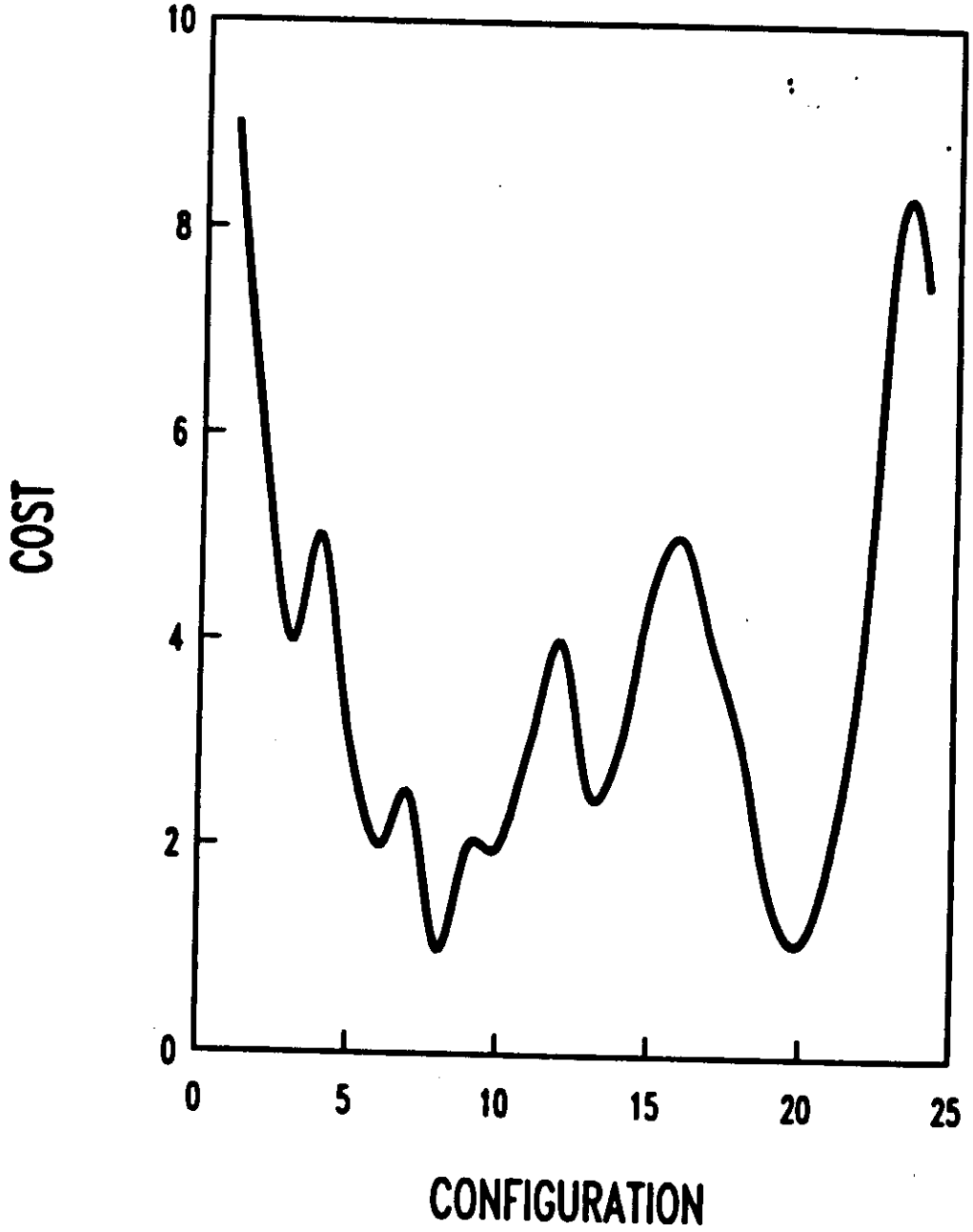


## Objective Function for Placement

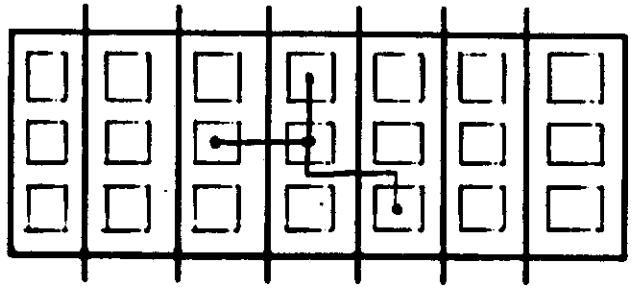

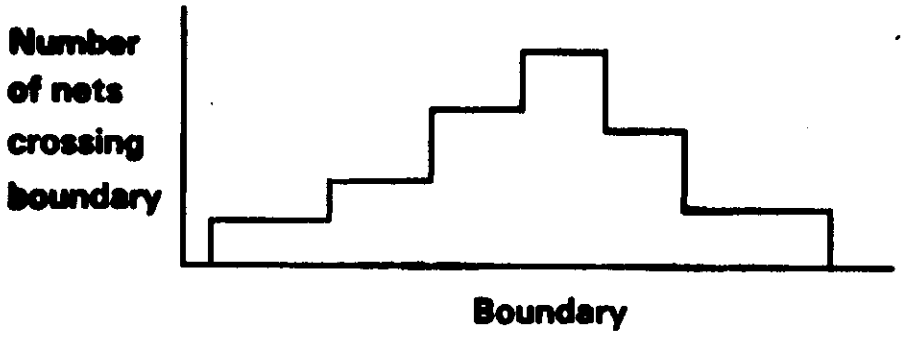


area under curve = horizontal net length

peaks measure congestion

Objective function:

f( line length, peaks )

CDG

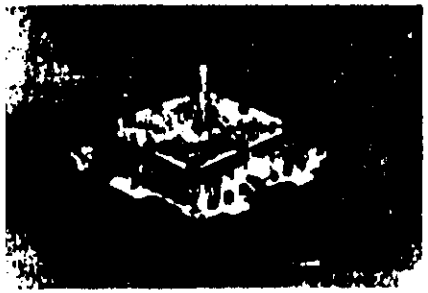

Figure 1 The thermal conduction module (TCM).

istons contact the back of each chip and provide the main hermal path to the water-cooled housing. A C-ring, lamped between the cover and a flange which is brazed to he substrate, seals the assembly.

*Multilayer ceramic substrate*

The 90-mm substrate (see the cross section shown in Fig. 4) onsists of up to 33 molybdenum metallized alumina layers hich are required for power distribution, for impedance-ontrolled interconnection of up to 12 000 chip pads, and for iring to the [redacted] A typical substrate contains 50 000 vias for layer-to-layer connections and 130 m of x-y iring. The total substrate thickness is approximately 5.5 m.

The ceramic formulation, consisting of approximately 0% alumina and 10% glass, was selected considering trength requirements, sintering characteristics, and shrink-ge compatibility with the molybdenum metallurgy.

A key design feature is the routing of all signal connec-ions from the chip (0.25-mm centers), through the upper-most layers in the substrate, to an array of surface pads, hich in turn are connected to internal wiring layers. This lesign (Fig. 5) provides the ability to delete connections to nternal layers by deleting a connection on the top surface nd to substitute a surface discrete wire when a wiring hange is needed. The discrete wires are ultrasonically onded to the gold-plated pads.

The center layers of the substrate inclu[redacted] rranged in x-y pairs to maximize wiring efficiency. Metal-ized, 0.12-mm-diameter vias on 0.5-mm centers are used for -plane-to-y-plane connections. Voltage reference planes are ppropriately interspersed for signal wiring impedance ontrol.

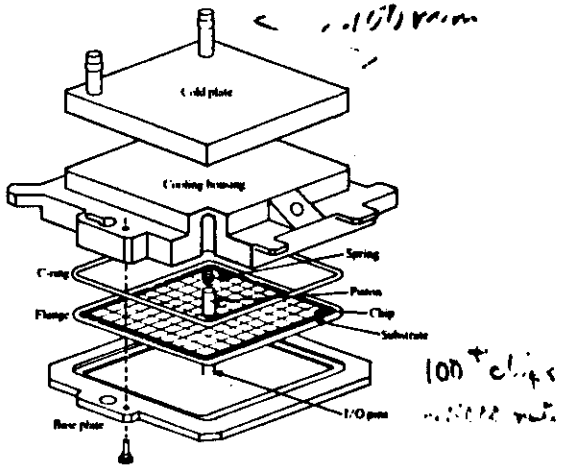


Figure 2 Exploded view of the TCM assembly.

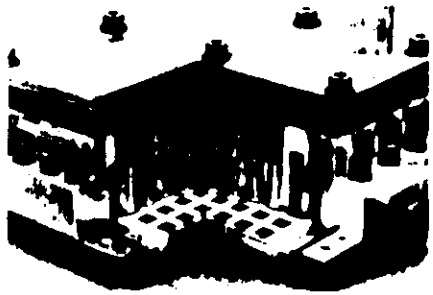

Figure 3 Cross section of the TCM.

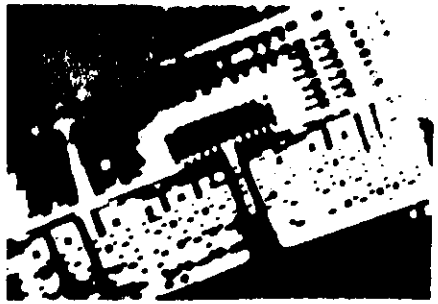

Figure 4 Cross section of a multilayer ceramic substrate.



from 3081:

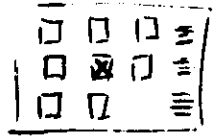

X = I/E unit

INITIAL POSITION: (existing Land placement)

| | | | | | | | | | | |
|---|---|---|---|---|---|---|---|---|---|---|
| | 1 | 2 | 3 | 4 | 5 | 6 | 7 | 8 | 9 | 10 |
| 262 | 11 | 12 | 13 | 14 | 15 | 16 | 17 | 18 | 19 | X |
| 421 | 21 | 22 | 23 | 24 | 25 | 26 | 27 | 28 | 29 | 30 |
| 613 | 31 | 32 | 33 | 34 | 35 | 36 | 37 | 38 | 39 | 40 |
| 824 | 41 | 42 | 43 | 44 | 45 | 46 | 47 | 48 | 49 | 50 |
| 826 | 51 | 52 | 53 | 54 | 55 | 56 | 57 | 58 | 59 | 60 |
| 797 | 61 | 62 | 63 | 64 | 65 | 66 | 67 | 68 | 69 | 70 |
| 662 | 71 | 72 | 73 | 74 | [redacted] | | | 78 | 79 | 80 |
| 356 | 81 | 82 | 83 | 84 | [redacted] | | 87 | [redacted] | 89 | 90 |
| 366 | 91 | 92 | 93 | 94 | 95 | [redacted] | 97 | 98 | 99 | [redacted] |
| | 306 | 428 | 555 | 759 | 879 | 945 | 898 | 672 | 210 | |

Illustrative example - 98 chips on 100 site ceramic module

~5000 connections
3000 nets
7000 pins

INITIAL POSITION:

T = 10000

| | | | | | | | | | | |
|---|---|---|---|---|---|---|---|---|---|---|
| 558 | 5 | [illegible] | 20 | 53 | 52 | 19 | 45 | 46 | 22 | 21 |
| 944 | 78 | 23 | 64 | 95 | 41 | 100 | 14 | 81 | [illegible] | 36 |
| 1193 | 26 | 70 | 16 | 91 | 8 | 31 | 9 | 43 | 55 | 62 |
| 1378 | 25 | 33 | 15 | 83 | 38 | 34 | 65 | [illegible] | 17 | 54 |
| 1388 | 68 | 57 | 48 | 84 | 79 | [illegible] | 13 | [illegible] | 50 | 87 |
| 1375 | 6 | 39 | 90 | 97 | 94 | 11 | 58 | 89 | 27 | 37 |
| 1170 | 69 | 98 | 55 | 63 | 10 | 67 | 72 | 66 | 44 | 60 |
| 838 | 7 | 80 | 73 | 30 | 29 | 69 | [illegible] | 47 | 49 | 4 |
| 436 | 3 | 24 | 61 | [illegible] | 51 | 18 | 32 | 35 | 1 | 2 |
| | 82 | 59 | 93 | 74 | 12 | 28 | 99 | 92 | 71 | 40 |

513 920 1091 1266 1369 1327 1147 858 503

T = 1250 :

| | | | | | | | | | | |
|---|---|---|---|---|---|---|---|---|---|---|
| 568 | 99 | 98 | 50 | 92 | 83 | 54 | 72 | 63 | 42 | 81 |
| 760 | 93 | 95 | 55 | 84 | 52 | 25 | 32 | [illegible] | 22 | 82 |
| 809 | [illegible] | 97 | 69 | 71 | [illegible] | 64 | [illegible] | 62 | 61 | 43 |
| 700 | 90 | 53 | 87 | [illegible] | [illegible] | [illegible] | 94 | 73 | 47 | 31 |
| 718 | 20 | 89 | 27 | 67 | 78 | 21 | 23 | 12 | 10 | 11 |
| 717 | 29 | 41 | 15 | 16 | 1 | 91 | 2 | 80 | 33 | 4 |
| 785 | 51 | 50 | 17 | 30 | 49 | 35 | 44 | 65 | 74 | 100 |
| 695 | 28 | 18 | 79 | 5 | 13 | 36 | 25 | 46 | 45 | 66 |
| 499 | 9 | 39 | 60 | 19 | 26 | 37 | 14 | 58 | 38 | 34 |
| | 3 | 6 | 8 | 7 | 57 | 56 | 70 | 59 | 68 | 48 |

477 700 892 782 820 932 909 736 489

T=0

final position

| | | | | | | | | | | |
|---|---|---|---|---|---|---|---|---|---|---|
| 485 | 71 | 92 | 93 | 94 | 87 | 63 | 62 | 42 | 43 | 28 |
| 563 | 83 | 84 | 97 | [redacted] | | 73 | 72 | 81 | 31 | 22 |
| 559 | 95 | 99 | 98 | [redacted] | | 52 | 61 | 32 | 12 | 23 |
| 560 | 5 | 15 | 90 | [redacted] | | | 82 | 14 | 13 | 2 |
| 591 | 16 | 25 | 78 | 55 | 69 | 10 | 3 | 21 | 11 | 1 |
| was 826 → 595 | 79 | 89 | 27 | 67 | 53 | 64 | 74 | 54 | 45 | 4 |
| 562 | 8 | 19 | 18 | 29 | 49 | 57 | 39 | 17 | 66 | 24 |
| 558 | 6 | 32 | 80 | 60 | 51 | 65 | 48 | 98 | 35 | 44 |
| 395 | 7 | 9 | 50 | 76 | 41 | 68 | 26 | 97 | 58 | 34 |
| | 30 | 28 | 100 | 69 | 91 | 36 | 37 | 38 | 56 | 33 |
| | 373 | 471 | 569 | 613 | 588 | 625 | 632 | 598 | 334 | |

was 946

250,000 interchanges attempted

8 min (3033) cpu

30% decrease in congestion

10% " " wire length

⇒ fewer overflow wires

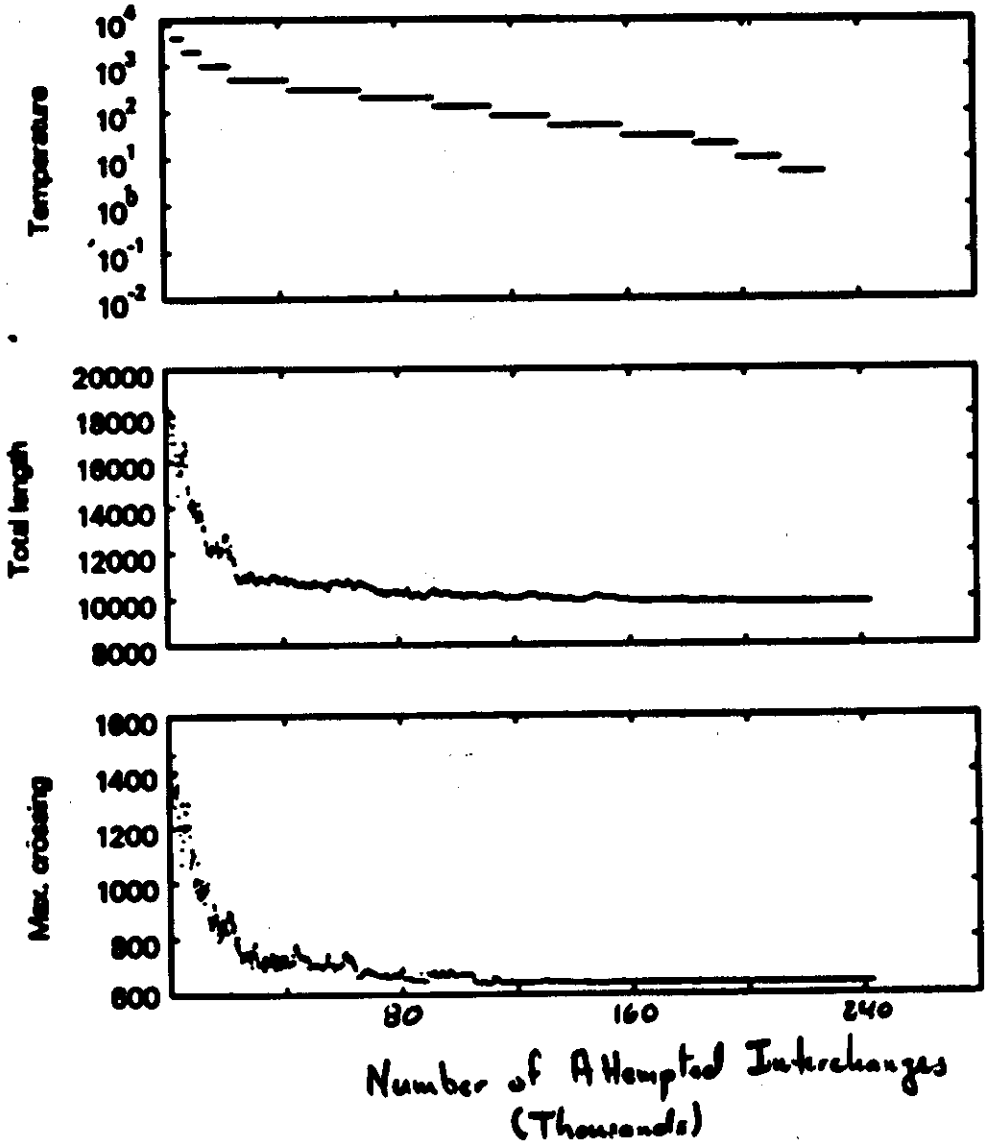


256,000 attempted: 12 min cpu (IBM 3033)

# Annealing Schedules

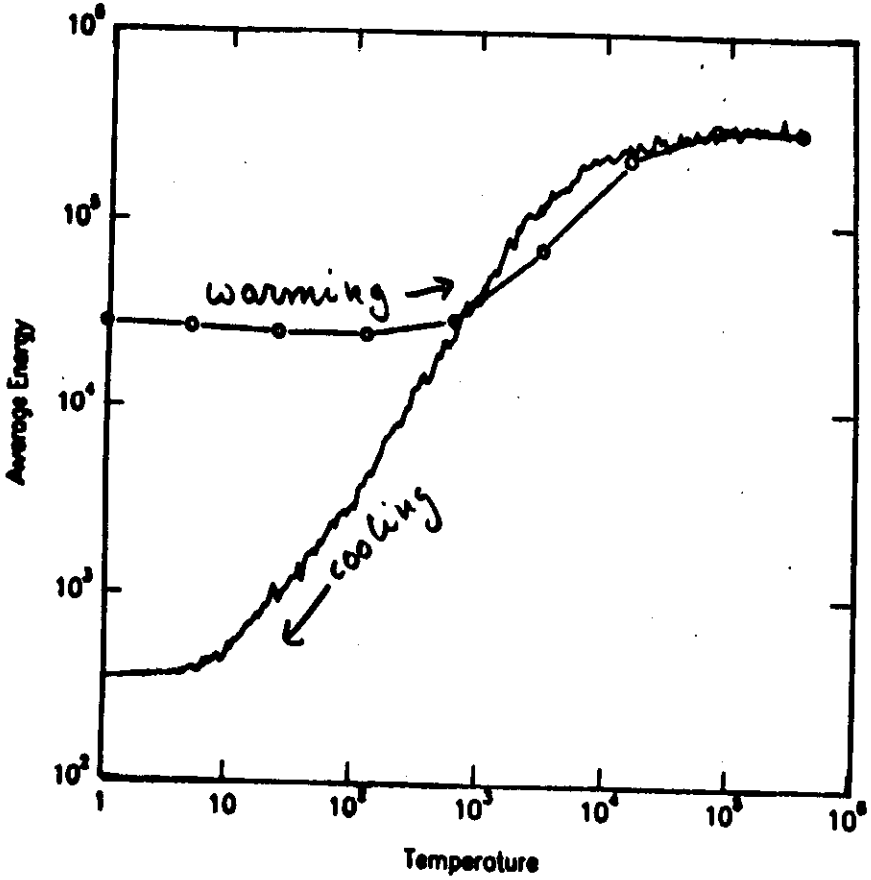


Average Energy versus Temperature for a Monte Carlo Placement.
(Data are from RADC95.3 CONYKT.)

S.R.White

Bibliography: Simulated Annealing

Kirkpatrick, Gelatt and Vecchi, Scienc 220, 671 (1983)

Vecchi and Kirkpatrick, IEEE Trans. on Computer Aided Design, CAD-2 #4, 215 (1983)

S. Kirkpatrick, J. Stat. Phys. 34, 975 (1984)

S. R. White, The Physics of VLSI, 261, AIP, (1984)

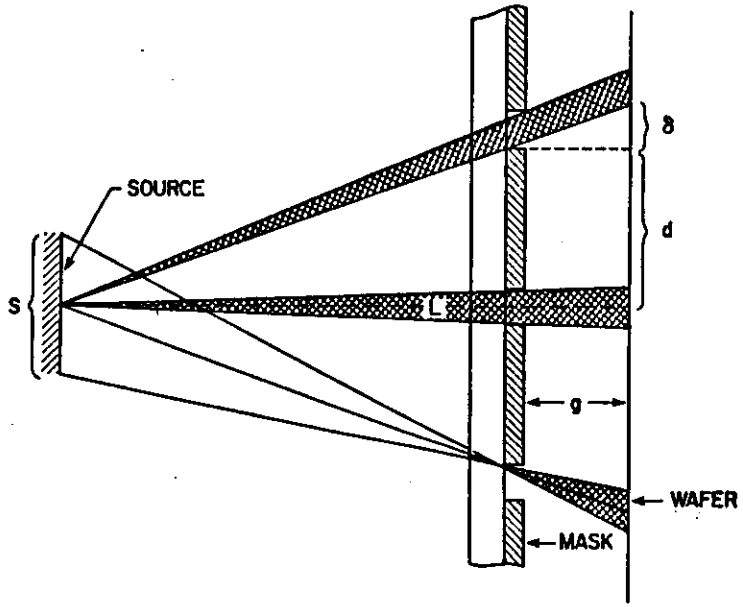


TABLE II: LITHOGRAPHY PARAMETERS FOR SEVERAL X-RAY SOURCES

| Source | L cm | d cm | S mm | ρ μm | δ μm | Flux* mW/cm² | Δδ μm |
|---|---|---|---|---|---|---|---|
| Electron impact | 20 | 2 | 2 | .5 | 5 | 1 | .5 |
| Laser plasma | 20 | 2 | 0.02 | .005 | 5 | 10 | .5 |
| Synchrotron | 1000 | 2 | <2 | <.01 | .1 | >200 | 0 |

* Source flux is estimated on "high side" for first two sources

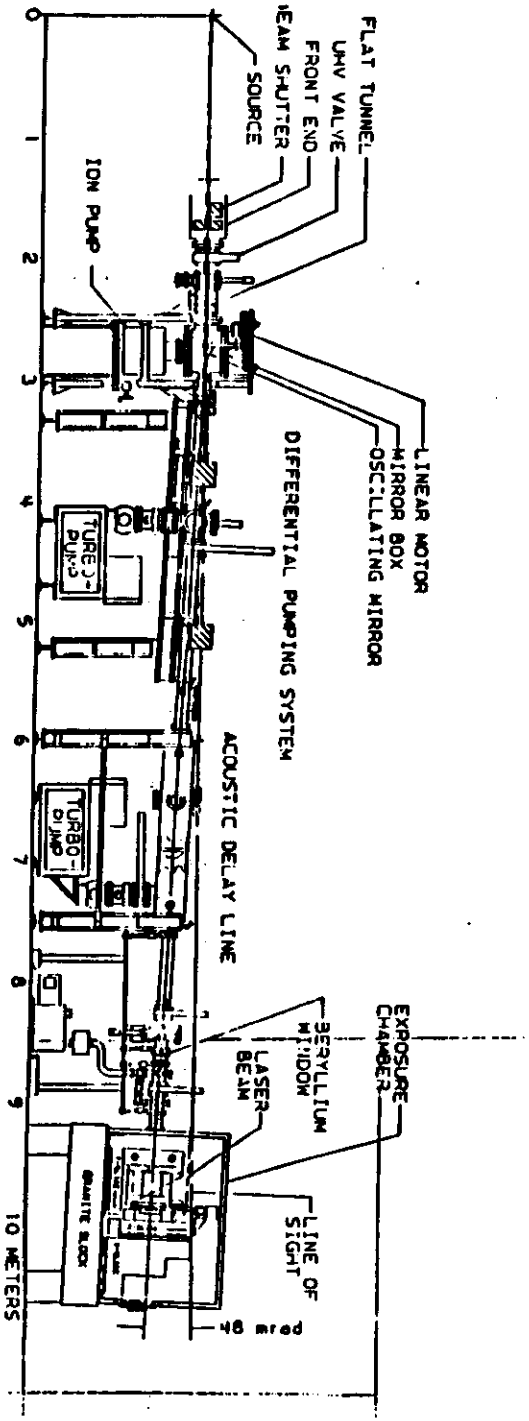

1. Deposit film (LPCVD)

2. Pattern back-side (RIE)

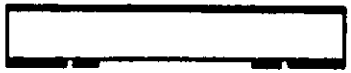

3. Etch silicon substrate
   - (KOH, anisotropic)
   - (HNA, isotropic)

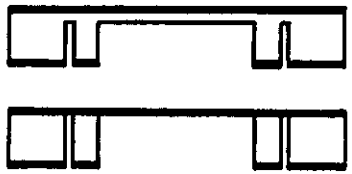

4. Bond to pyrex ring

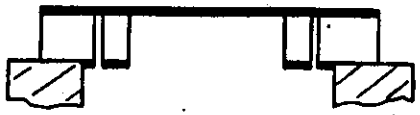

TABLE IV: STORAGE RING PARAMETERS

| Ring* | $\lambda_c$ Å | E GeV | <I> ma | EI GeV-ma | C m |
|---|---|---|---|---|---|
| LISO1I | 10 | 1 | 200 | 200 | 18 |
| NSLS-VUV | 25 | .75 | 400 | 300 | 47 |
| BESSY | 20 | .8 | 400 | 320 | |
| COSYI | 20 | .43 | ~100 | 43 | 2.4 |
| COSYII | | | | | |
| 1 | 10 | .68 | 200 | 136 | |
| 2 | 5.5 | .9 | 100 | 90 | ~ 6-10 |
| 3 | 10 | .68 | 200 | 136 | |
| 4 | 15.3 | .9 | 2-300 | 180-270 | |

* LISO1I = IBM consultant designed ring; NSLS-VUV = Brookhaven ring we are using; BESSY = Berlin electron storage synchrotron-site of major Europe x-ray lithography project; COSYI = first German compact superconducting storage rings; COSYII = compact rings designed (limited) for IBM by vendors/consultants.

TABLE I: COMPLEXITY OF SEMICONDUCTOR INTEGRATED CIRCUITS

| YEAR | CLASS* | NO. DEVICES | | LITHO (μm) | CHIP SIZE $mm^2$ | WAFER SIZE mm |
|---|---|---|---|---|---|---|
| 60-68 | SSI | $2^1 - 2^7$ | (2 - 128) | > 10 | 1-15 | 25 |
| 65-75 | MSI | $2^6 - 2^{12}$ | (64 - 4K) | 3 - 10 | 10 - 25 | 50 |
| 72-83 | LSI | $2^{11} - 2^{17}$ | (20K - 128K) | 1.5 - 4 | 15 - 50 | 50 - 100 |
| 80-88 | VLSI | $2^{16} - 2^{22}$ | (64K - 4M) | .75 - 2 | 25 - 75 | 100 - 125 |
| 85-93 | GSI | $2^{21} - 2^{27}$ | (2M - 128M) | .5 - 1 | 50 - 200 | 125 - 200 |
| 90-99 | HSI | $2^{26} - 2^{32}$ | (64M - 4000M) | ≤.5 | 100 - 400 | ≥ 200 |

* SSI = Small Scale Integration, MSI = Medium Scale Integration, LSI = Large Scale Integration, VLSI = Very Large Scale Integration, GSI = Giant Scale Integration, HSI = Horrendous Scale Integration



## JOSEPHSON CHRONOLOGY

| | |
|---|---|
| 1962 | JOSEPHSON PAPER |
| 1965 | MATISOO PH.D., JOINS IBM |
| 1966 | FIRST SWITCHING RESULTS PUBLISHED |
| 1969-70 | APPLIED RESEARCH STUDY |
| 1970 | MATISOO JOINS APPLIED RESEARCH |
| 1972 | JOSEPHSON JUNCTION MAJOR PROGRAM |

Reprinted from
Volume 9, Number 4 APPLIED PHYSICS LETTERS 15 August 1966

# SUBNANOSECOND PAIR-TUNNELING TO SINGLE-PARTICLE TUNNELING TRANSITIONS IN JOSEPHSON JUNCTIONS

*J. Matisoo*
IBM Watson Research Center
Yorktown Heights, New York
(Received 4 April 1966; in final form 25 July 1966)

This Letter reports the measurement of an upper bound of 0.8 nsec for the time of transition of Sn-$SnO_x$-Sn Josephson junctions from the pair tunneling ($V = 0$) to the single-particle tunneling state ($V = 2\Delta$: 1mV at 1.7°K). The threshold is extremely sharp. There is no observed delay in the transition after the threshold is exceeded, and there is no change in the observed risetime of the signal with changes in driving current amplitude or risetime. The magnetic field behavior of these junctions is the same as that observed in the dc case. The combination of high speed, sharp threshold, and strong magnetic field dependence are desirable properties for logic elements.

We report below the measurement of an upper bound of 0.8 nsec for the time of transition of Sn-$SnO_x$-Sn Josephson junctions from the pair tunneling to the single-particle tunneling state. This bound is imposed by the characteristics of the measuring circuit. The actual transition time may be substantially smaller.

A Josephson junction consists of two superconductors separated by a barrier (usually an oxide of one of the superconductors) which is sufficiently thin so that the superconductors are weakly coupled.[1-3] The coupling is such that below some maximum amplitude, zero-voltage current can flow, i.e., the barrier also behaves as a superconductor. The coupling is broken when the maximum current is exceeded. If circuit constraints are such that current must remain constant, a transistion is made from this zero-voltage state to the single-particle tunneling state which has the same current. In the case considered below, the voltage across the junction in this state is $2\Delta$, where $\Delta$ is the energy gap.

The Sn-$SnO_x$-Sn junctions were prepared by evaporating tin through a mask in a vacuum of $10^{-6}$ mm Hg. In this way a tin line of 0.13 mm width is formed which is subsequently oxidized in the atmosphere for 1 hr. The second tin line is then evaporated so that 0.13 mm overlaps with the previously deposited (and oxidized) line. The result is a 0.13 mm × 0.13 mm junction. The length of the samples is 0.5 cm. Under the junction and insulated from it is a lead ground plane. The ground plane serves to minimize the inductance of the lines which would adversely affect the measurements. (The inductance of the sample is $5 \times 10^{-11}$ h). The leads for measuring voltage across the junction are silver. Electrical contact to coaxial cable is made through beryllium copper spring contacts tipped with tin spheres. The tin spheres press into soft indium (smeared on the silver lands) assuring stable contact. These junctions typically have zero-voltage currents of 1 mA at 1.7°K, the usual temperature of measurement.

The measurement system is shown schematically in Fig. 1. The method of measurement is to make the Josephson junction the termination of a transmission line. Since the resistance of the tunnel junction even in the single-particle tunneling state is much less than the 50 Ω characteristic impedance of the transmission line, the current through the junction is essentially constant for the duration of the pulse (and is $\sim 2V/Z_0$, where $V$ is the amplitude of the pulse). The measured risetime (10% – 90%) of the pulse generator is 0.7 nsec, however, it is not the limiting risetime of the measuring apparatus. The risetime is limited to 0.8 nsec by the inductance of the copper springs and the dispersion in the microdot cable. (Note that the inductance of the

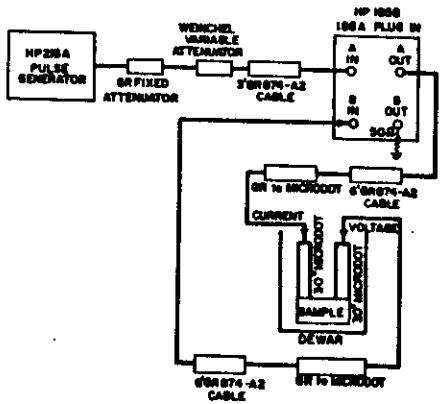


Fig. 1. Block diagram of apparatus used for measurements.





0.13 mm wide line of 0.5 cm length is $5 \times 10^{-11}$ h so $L/Z_0 \cong 10^{-12}$ sec).

Figure 2 shows traces immediately below and above the threshold. Since $2\Delta$ for Sn at 1.7°K is approximately 1 mV the signal amplitude is 1 mV. The observed risetime of the signal is 0.8 nsec. Thus the transition time is $\leq$ 0.8 nsec. It is found that the threshold is extremely sharp in the sense that very small (< 0.1 dB) changes in pulse amplitude at the threshold will maintain the junction either in the pair-tunneling state, in which there is no voltage across the junction, or in the single-particle tunneling state in which there is a voltage drop equal to $2\Delta$. There is no observed dependence of the threshold on pulse repetition rate (1 MHz for these measurements). More significantly, there is no observed delay in the transition after the threshold is exceeded and there is no change in the observed risetime of the signal with changes in driving current. The magnetic field behavior of these junctions is the same as that observed in the dc case; i.e., they exhibit the typical diffraction pattern.[4]

The transition from the single-particle to the pair-tunneling state can also be observed. The transition to the pair-tunneling state begins when the current through the junction falls to the value at which the voltage across the junction is $\Delta$. Since this occurs during the fall time of the pulse the signal can be obscured by derivating noise. (The same problem does not occur on transition from pair- to single-particle tunneling because of the sharpness of the threshold. Since the pulse amplitude variations are greater than 0.1 dB, the transition can be adjusted to occur after the derivative noise has died out.) However, for junctions with ground planes and small critical currents the measurement can be made accurately. The total time required for the voltage to fall from $V = 2\Delta$ to zero is approximately 2 nsec. Since approximately 1 nsec is pulse fall time, the transition occurs in approximately 1 nsec or less. (This again, is an upper bound set by the measuring apparatus).

Fig. 2. Oscilloscope trace showing voltage across the Sn-$SnO_x$-Sn junction below threshold (lower trace) and the transition from pair-tunneling state to single-particle tunneling state. Horizontal calibration: 0.4 nsec/cm; vertical calibration: 1 mV/cm. $H_{\text{normal}} = 0$; $T = 1.7$°K.

No systematic variation of parameters has been performed, but the bound of 0.8 nsec on the transition time is independent of a change in junction area by a factor of four, change in the driving pulse risetime by an order of magnitude (1 nsec–15 nsec), and changes in barrier thickness; i.e., from critical currents of 1 mA to 50 mA. The determination of parameter dependence must await construction of apparatus of better time resolution which is in progress.

Similarly, no theoretical calculation of transition speed is possible at present, since a theory which describes the time dependence of breakdown of phase coherence does not exist. (Note that the Josephson equations do not describe this process).

In summary, Josephson junctions are observed to switch from the pair-tunneling state to the single-particle tunneling state and vice versa in less than one nsec. The actual transition times may, in fact, be considerably smaller.

It is clear that these transition times are considerably shorter than those measured for thin film cryotrons (10–40 nsec).[5,6]

The combination of high speed, sharp threshold, and strong magnetic field dependence makes Josephson junctions attractive as logic elements.

I thank Robert T. Chase for fabricating the junctions.

[1] B. D. Josephson, *Phys. Letters* **1**, 251 (1962).
[2] B. D. Josephson, *Rev. Mod. Phys.* **36**, 216 (1964).
[3] P. W. Anderson and J. M. Rowell, *Phys. Rev. Letters* **10**, 230 (1963).
[4] J. M. Rowell, *Phys. Rev. Letters* **11**, 200 (1965).
[5] J. I. Gittleman and S. Bozowski, *Phys. Rev.* **135**, A297 (1964).
[6] A. E. Brennemann, J. J. McNichol and D. P. Seraphim, *Proc. IEEE* **51**, 1009 (1965).

# HE TUNNELING CRYOTRON—A SUPERCONDUCTIVE LOGIC ELEMENT BASED ON ELECTRON TUNNELING

BY
J. MATISOO

*Reprinted from the* PROCEEDINGS OF THE IEEE
VOL. 55, NO. 2, FEBRUARY, 1967
pp. 172-180




## JOSEPHSON RESULTS

- CHIPS AND PACKAGE DEVELOPED AND CROSS SECTION OF COMPUTER PROCESSOR BUILT
- FIND MEMORY LESS FORGIVING THAN LOGIC DESIGN. TOLERANCES NOT ADEQUATE TO SUPPORT HIGH PERFORMANCE MEMORY.
- NO INCREMENTAL APPLICATION AVAILABLE
- CAN BUILD SYSTEM 2-5 TIMES FASTER THAN WITH Si BUT JUDGED NOT GOOD ENOUGH
- PROGRAM TERMINATED IN 1984

1966: First demonstration of 2-Dimensionality in Inversion Layers - Fang, Fowler Howard, Stiles

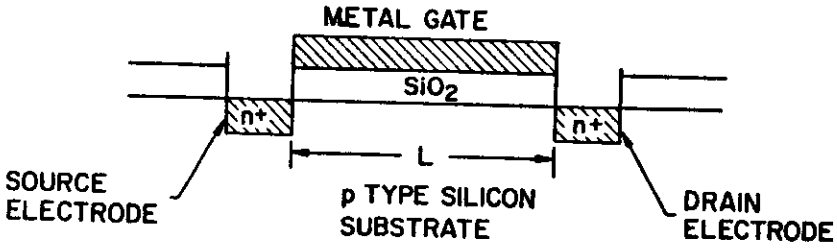


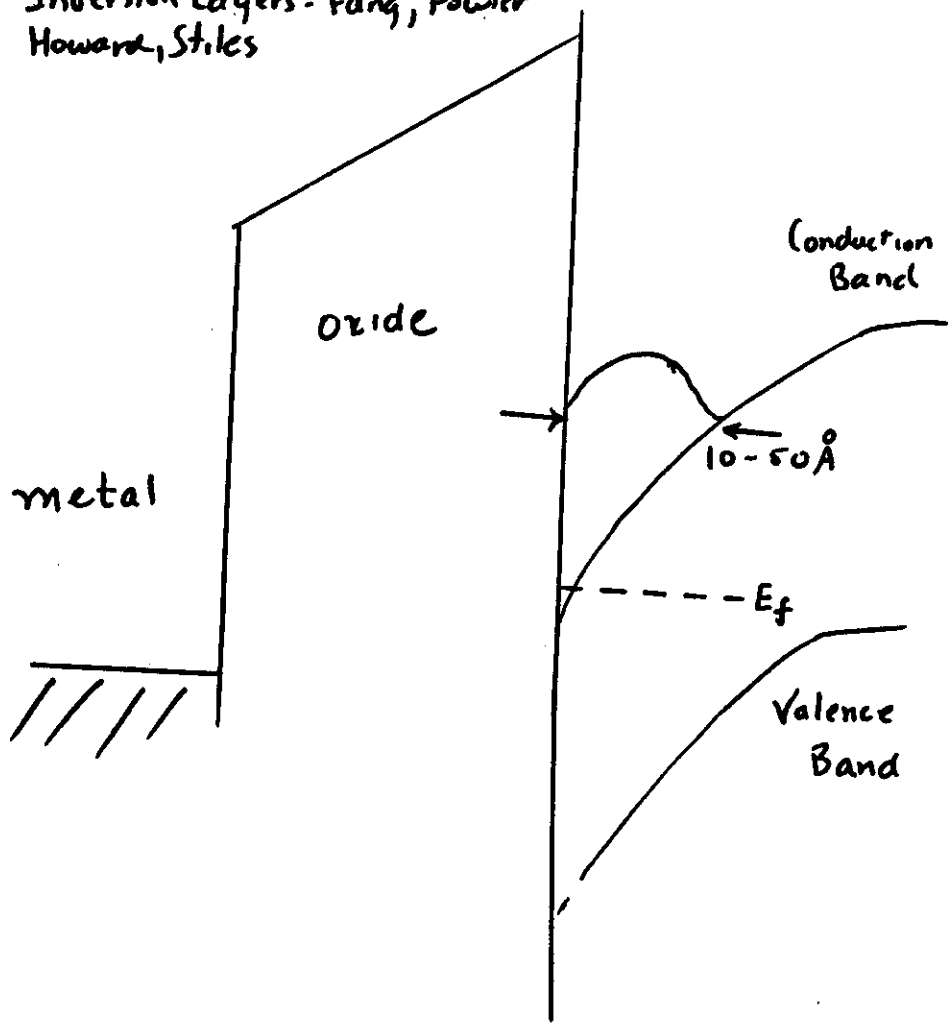

(a)
(b)
(c)
(d)
DEPLETION WIDTH
$E_V$
$E_A$
$E_F$
$E_C$


3777 T
33 kOe
1.34°K
CONDUCTANCE
0
20
40
60
80
100
GATE VOLTAGE

# Electrons in Silicon Microstructures

R. E. HOWARD, L. D. JACKEL, P. M. MANKIEWICH, W. J. SKOCPOL

**Silicon microstructures only a few hundred atoms wide can be fabricated and used to study electron transport in narrow channels. Spatially localized voltage probes as close together as 0.1 micrometer can be used to investigate a variety of physical phenomena, including velocity saturation due to phonon emission, the local potentials caused by scattering from a single trapped electron, and quantum tunneling or hopping among very few electron states.**

THE PRODUCTION OF INTEGRATED CIRCUITS INVOLVES some of the most sophisticated and precise manufacturing techniques ever developed and uses raw materials with an unmatched degree of purity and perfection. For example, single-crystal silicon wafers 15 cm or more in diameter can be obtained with concentrations of undesired dopants at less than one part in 10 billion and with only about one defect per square centimeter. Dimensional tolerances for film thicknesses used in this technology are routinely held to an accuracy of a few nanometers, and feature sizes in commercial circuits are already as small as 1 μm and will shortly be even smaller. The physics and chemistry of silicon, as well as its surfaces and interfaces with many materials, are exceptionally well understood. The electronic band structure and transport properties have also been extensively studied in an effort to gain greater insight into the behavior of this important material and devices made from it.

This combination of chemical and crystal perfection, coupled with a thorough understanding of the basic material and devices, makes silicon transistors attractive model systems for investigating a variety of fundamental problems, particularly electron transport in solids. New patterning techniques now exist for making devices with features nearly 100 times smaller than those used in commercial integrated circuits (*1*, *2*). These techniques can be combined with the well-characterized semiconductor technology to manufacture devices that make it possible to study transport physics in microstructures only a few hundred atoms across.

The device used for these studies is the metal-oxide-semiconductor field-effect transistor (MOSFET), the cornerstone of much of the conventional silicon integrated-circuit technology. In this article, we describe these transistors and how they can be used to make a variety of fundamental measurements. These include studying the velocity-field relation for electrons, the scattering effects of one charged defect, and the characteristics of quantum mechanical hopping between individual electron states.

## MOS Transistors

In the large MOSFET's common in commercial microchips, the current is through an electron layer that behaves like a quantum mechanically two-dimensional gas (*3*). For nearly two decades, the special properties of this two-dimensional electron system have b investigated, leading to such discoveries as the quantum Hall ef (*4*).

Figure 1 shows the schematic structure of a single M transistor, designed for use in the physics experiments descri below (*5*). It differs from typical MOSFET's only in the shap the metal gate (G). This gate is separated from the silicon subst by an insulating layer of silicon dioxide. Nearby, metal l [source (S) and drain (D)] make contact with electron-rich n- regions of the silicon ($n^+$). The rest of the silicon is $p$ - (conduction by holes), so that electrical conduction betw contacts is blocked by $p$-$n$ diodes. When a positive charge is ap to the metal gate, however, a thin layer of electrons from contacts is attracted into a potential well held tightly against oxide-silicon interface. This two-dimensional electron gas (i sion layer) has the same shape as the gate above it and can be to complete a circuit between the $n$-type contacts. Once threshold voltage for formation of an inversion layer is reache system is essentially a parallel-plate capacitor, with the el density in the inversion layer being equal and opposite t additional charge density on the gate. Thus the gate control electron density, and hence the conductivity, of the inversion between the contacts. The inversion layer is so tightly b against the interface that only the lowest quantized state of m perpendicular to the interface is energetically favorable, an occupied electron states differ only in their motion in the pl the interface (*3*). Hence, the motion is strictly two dimensi

*Narrow inversion layers.* Advances in microfabrication (*1*, *2* made possible the fabrication of MOS transistors with narro segments that control narrow conducting channels in the in ing silicon. This is shown in Fig. 1 where the central section gate has a segment of width W and length L with the el current in the inversion layer directed from the wide segme the source to the corresponding segment near the drain devices, with W much less than 1 μm, allow study of the properties of conduction in electron systems with an incre "one-dimensional" character (*6*–*18*). The geometry is part appropriate for transport experiments, since even a short s of a narrow channel can contribute an appreciable fractio electrical resistance between the contacts.

## A New Experimental Approach

What has been described so far is a conventional MOSFET, but with a gate made narrow so as to approx dimensional conduction path. In this section, we deac experiments with MOSFET's having gates of increased ge complexity in which spatially localized voltage measureme narrow channels are made on length scales of 100 nm. The are otherwise similar to those described earlier (*6*–*9*). Figu micrograph of a 60-μm square region on a silicon wafer c

The authors are in the Communications Sciences Division of AT&T Bell L Holmdel, NJ 07733.

SCIENCE





eight different implanted contacts and their associated metal leads. The bright pattern toward the center is metal on top of an $n$-type polysilicon gate electrode defined by electron-beam lithography and reactive ion etching (*1*, *2*). A 20-nm oxide layer separates this gate electrode from the underlying inversion layer of the same shape. The pattern converges in the center of the micrograph to microstructures so small that they are impossible to image in an optical microscope.

Figure 2B shows an electron micrograph of the central region at 100 times higher magnification. In this case, the pattern consists of a narrow conducting channel with side branches. An external power supply is connected between the source side (S) and the drain side (D) of the transistor, forcing electrons to flow through the conducting channel under the gate. High-impedance voltmeters can be attached to each of the non–current-carrying side branches to measure the local potential along the channel.

Figure 2C presents a perspective view of the same structure, showing that the relatively thin metal gate and side branches have been used as protective masks against reactive ion etching of the polysilicon, silicon dioxide, and the underlying silicon substrate. This process leaves behind a vertical-walled structure containing the inversion layer. Because oxide and silicon on either side have been removed, the inversion layer at the oxide-silicon interface is physically constrained to have the same shape as the gate above.

The ability to make spatially localized voltage measurements on the 0.1-μm scale by means of these devices can be useful in probing many different aspects of conduction by electrons in inversion layers. Although the density of electrons in an inversion layer is much less than that in a metal, the physics can be quite similar.

At the conventional textbook level, conduction in metals is limited at high temperatures by interactions between electrodes and quantized lattice vibrations (phonons). At low temperatures these are less frequent, and the resistance decreases until collisions with other electrons and with impurity atoms predominate. The residual impurity scattering is essentially temperature independent, and for years that was the end of the story. Recently, however, it has been realized that localization and many-body aspects of the quantum mechanical conduction result in previously unanticipated resistance increases at low temperatures (below about 4 K), particularly in disordered systems with reduced dimensionality (*19*).

All the effects described above are observable in MOSFET inversion layers, and spatially localized measurements can shed additional light on each.

## Experimental Applications of Microstructures

***Phonon-limited drift velocity.*** For the first of three experimental applications of these devices, let us consider the interactions of electrons with phonons, the dominant scattering mechanism at room temperature. As the electric field driving the current increases, electrons acquire a drift velocity superimposed on their usual motions. Also, the average electron energy increases, and the electrons become capable of emitting more phonons. This phonon emission eventually tends to limit the drift velocity of electrons in silicon inversion layers to values of order $10^7$ cm sec$^{-1}$. This effect has previously been studied by time-of-flight measurements over distances of order 60 μm (*20*) and has been inferred from the operating characteristics of conventional transistors.

With spatially localized probes, in situ measurement of velocity saturation due to phonon scattering is easily accomplished. The electric field is simply the voltage drop between adjacent probes divided by their spacing, and the drift velocity is defined as the current per unit width divided by the local charge density. As the current and field are increased, a voltage drop builds up along the conducting channel, and the positively biased end of the channel rises closer to the gate voltage, so that the electron density is smaller. By measuring the local channel potential, the charge density can be calculated with the use of few assumptions.

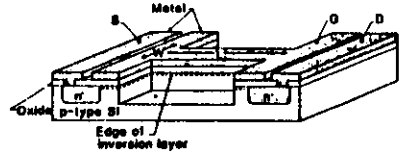


Fig. 1. Schematic diagram of a metal-oxide-semiconductor field-effect transistor (MOSFET). Conduction between the source (S) and drain (D) must pass through the thin electron inversion layer controlled by the gate (G). If the width W of the gate is narrow enough (of order 0.1 μm), conduction through the inversion layer displays an increasingly "one-dimensional" character.

Figure 3 shows the electron drift velocity as a function of electric field for a narrow conducting channel 0.12 μm wide, with voltage probes spaced 0.25 μm apart. The tendency of the drift velocity to

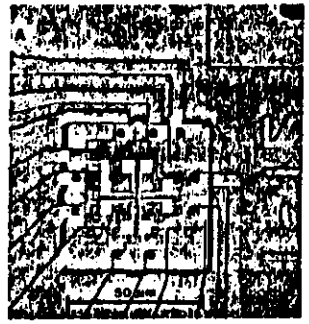


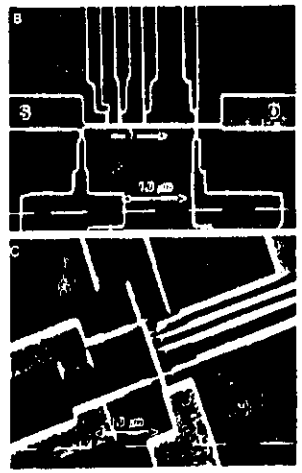


Fig. 2. Multicontact device structure for making spatially localized voltage measurements in a MOSFET. (A) Overview of a 50-μm contact region. (B) Electron micrograph of central region in which spatially localized voltage measurements are made. The narrow conducting channels are only several hundred atoms wide. (C) Perspective view of the same region, showing the etched pedestal that confines the narrow inversion layer.